

Inclusive Jet Production with Virtual Photons in Next-to-Leading Order QCD

M. Klasen¹, G. Kramer², B. Pötter²

¹ Deutsches Elektronen-Synchrotron DESY,
Notkestr. 85, D-22607 Hamburg, Germany,
e-mail: klasen@mail.desy.de

² II. Institut für Theoretische Physik*, Universität Hamburg
Luruper Chaussee 149, D-22761 Hamburg, Germany
e-mail: kramer@mail.desy.de, poetter@mail.desy.de

Abstract

We present a next-to-leading order calculation for the virtual photoproduction of one and two jets in ep collisions. Soft and collinear singularities are extracted using the phase space slicing method. The collinear photon initial state singularity depends logarithmically on the mass of the virtual photon and is absorbed into the virtual photon structure function. An $\overline{\text{MS}}$ factorization scheme is defined similarly to the real photon case. Numerical results are presented for HERA conditions using the Snowmass jet definition for inclusive single jet and dijet cross sections. We study the dependence of these cross sections on the transverse energies and rapidities of the jets. Finally, we compare the ratio of the experimentally defined resolved and direct cross sections with recent ZEUS data as a function of the photon virtuality P^2 .

*Supported by Bundesministerium für Forschung und Technologie, Bonn, Germany, under Contract 05 7 HH 92P (0), and by EEC Program *Human Capital and Mobility* through Network *Physics at High Energy Colliders* under Contract CHRX-CT93-0357 (DG12 COMA).

1 Introduction

In ep scattering at HERA interactions between photons of small virtuality P^2 and protons produce jets of high transverse energy E_T . The presence of this hard scale E_T allows the application of perturbative QCD to predict cross sections for the production of two or more high- E_T jets which can be confronted with experimental data. This offers the opportunity to test QCD and to constrain the structure of the colliding particles.

At leading order (LO) QCD two distinct processes are responsible for the production of jets. In the direct photon process, the photon interacts as a point-like object with a parton in the proton, whereas in the resolved process the photon acts as a source of partons which then scatter with the partons coming from the proton. Both LO processes are characterized by having two outgoing jets of large transverse energy. Studies of dijet photoproduction at HERA have shown that both classes of processes are present for the case of quasi-real photons, i.e. photons of extremely small virtuality $P^2 \simeq 0$ [1, 2]. The comparison of theoretical predictions [3, 4] with these [2] and more recent experimental data [5] have given us some confidence that the parton distribution functions for the real photon available in the literature [6] are consistent with the dijet production data. The parton content of photons with virtuality $P^2 = 0$ is reasonably constrained by data from deep inelastic scattering [7]. Unfortunately this is not the case for a photon target with non-zero, although small, virtuality P^2 . The only measurement for the virtual photon structure function available so far has been performed by the PLUTO collaboration at PETRA [8]. They measured the structure function $F_{eff} = F_2 + \frac{3}{2}F_L$ for $P^2 \leq 0.8 \text{ GeV}^2$ and $Q^2 = 5 \text{ GeV}^2$ as a function of x (Q^2 is the virtuality of the probing virtual photon, whereas P^2 always denotes the virtuality of the probed virtual target photon). More and better data should come from LEP2 [9]. On the theoretical side several models exist for describing the Q^2 -evolution equations of the parton distributions and the input distributions at Q_0 with changing P^2 [10, 11, 12]. These constructions use essentially the same methods as have been applied for the parton distributions of real photons. This way some smooth behavior towards $P^2 = 0$, where previous results for the real photon should hold, is guaranteed. In [10] this construction allows a calculation of the parton distribution functions (PDF) for virtual photons in LO and NLO. It incorporates a purely perturbative contribution and a non-pointlike hadronic contribution. Unfortunately these PDF's for $P^2 \neq 0$ are not available in a form that parametrizes the Q^2 evolution. Such parametrized PDF's for virtual photons have been presented recently by two groups [11, 12], but unfortunately only in LO. These two models differ somewhat in their method of extrapolation to $P^2 \neq 0$, in the choice of the input distribution and the choice of the input scale Q_0 . Furthermore the PDF's of Glück, Reya and Stratmann (GRS) [12] present distributions only for $N_f = 3$ flavors, whereas Schuler and Sjöstrand (SaS) give PDF's for $N_f = 4$ flavors [11]. We expect these two structure function sets to be detailed enough so they can be tested in photoproduction experiments with virtual photons. First preliminary data have been presented by the ZEUS [15] and the H1 [16] collaborations. ZEUS studied the dijet cross section for $E_T > 4 \text{ GeV}$ in the range of $0 < x_\gamma < 1$. Events with $x_\gamma > 0.75$ are assumed to be dominated by the direct process whereas events with

$0 < x_\gamma < 0.75$ give the resolved component. Then the ratio of the direct-enriched and resolved-enriched cross section is measured as a function of P^2 for $0 < P^2 < 0.55 \text{ GeV}^2$. In the H1 experiment the inclusive one-jet cross section is measured as a function of E_T and rapidity η for various P^2 bins [16]. It is expected that the resolved component decreases relative to the contribution from the direct photon processes as the virtuality of the photon increases. Some theoretical studies of the single inclusive and dijet inclusive cross section in LO have been presented recently [12, 13, 14].

It is well-known that in NLO calculations the distinction between direct and resolved photoproduction becomes ambiguous. In this order, a large contribution in the NLO direct cross section is subtracted from the direct component and combined with the LO resolved term thus producing the scale ($Q \equiv M_\gamma$) dependence of the PDF's of the photon. Therefore both components are related to each other through the factorization scale M_γ at the photon leg which determines the part of the NLO direct contributions to be absorbed into the resolved component. The M_γ dependence of the remaining NLO direct contribution cancels to a large extent against the dependence in the resolved cross section coming from the photon structure function. This connection has been worked out in detail [17, 4] and studied numerically for real photoproduction with $P^2 = 0$ [18]. It is clear that this cancellation of the scale dependence must take place also for $P^2 \neq 0$. So, for a consistent calculation up to NLO one needs to superimpose both contributions, the NLO direct and at least the LO resolved cross section, both computed with the same scale. The subtraction of the large contribution in the direct cross section which is shifted to the resolved term is defined only up to finite, non-singular terms in the limit $P^2 \rightarrow 0$. These finite terms may be fixed in a way that a smooth behavior towards the limiting case of real photons ($P^2 = 0$) is achieved where these finite terms are usually defined in the $\overline{\text{MS}}$ subtraction scheme. For a complete NLO calculation we must include the NLO hard scattering parton-parton cross sections for the direct (here one of the ingoing partons is the photon with virtuality $P^2 \neq 0$) and for the resolved process together with the two-loop evolved structure function of the proton and photon with virtuality $P^2 \neq 0$.

In this paper we shall work out the subtraction in the NLO direct contribution and superimpose the remaining direct contribution and the resolved cross section up to NLO. We study this cross section and the two contributions as a function of P^2 for various inclusive one- and two-jet cross sections. Of particular interest is the behavior of the resolved component as a function of P^2 and the question at which P^2 the sum of direct and resolved cross sections approaches the unsubtracted direct cross section which one expects to give the correct description at sufficiently large P^2 .

The outline is as follows. In section 2 we describe how to subtract the singular terms in the NLO direct cross section connected with the collinear singularity of the $\gamma \rightarrow q\bar{q}$ contribution. Here we also define the finite terms which depend on the subtraction scheme used for $P^2 = 0$. Our result concerning the P^2 dependence of various one- and two-jet cross sections are presented in section 3. In this section we also compare with the preliminary data from ZEUS [15]. Section 4 contains a summary and an outlook for future investigations.

2 Subtraction of Photon Initial State Singularities

The NLO corrections to the direct process become singular in the limit $P^2 = 0$. For real photoproduction these photon initial state singularities are usually evaluated, i.e. regularized, with the dimensional regularization method in which they are finite for $\epsilon = (4 - d)/2$. The singular contributions appear as poles in ϵ multiplied by the splitting function $P_{q_i \leftarrow \gamma}$ [19]. These initial state singularities are absorbed into the PDF of the real photon ($P^2 = 0$). With no further finite terms subtracted (for $\epsilon \rightarrow 0$) this defines the $\overline{\text{MS}}$ factorization scheme which must be consistently applied also for the NLO evolution of the photon PDF. For $P^2 \neq 0$ the corresponding contributions appear as terms proportional to $\ln(P^2/s)$, \sqrt{s} being the c.m. energy of the photon-parton subprocess. These terms are finite as long as $P^2 \neq 0$ and can be calculated with $d = 4$ dimensions. Since for small P^2 these terms are large they are absorbed as in the case $P^2 = 0$ into the PDF of the virtual photon which is present in the resolved cross section. Concerning finite terms (for $P^2 \rightarrow 0$) which may also be subtracted together with the singular terms we have the same freedom as in the case $P^2 = 0$. We fix these finite terms such that they agree with the $\overline{\text{MS}}$ factorization in the real photon case. To achieve this we must compare the contributions originating from the photon initial state singularities in the two cases $P^2 = 0$ and $P^2 \neq 0$, which we shall do in the following.

For this purpose we must isolate the singular terms from the photon initial state when the photon is collinear with one of the outgoing quarks or antiquarks. The relevant processes are labeled K_1, K_2, K_3 and K_4 as specified in Tab. 1. We do not separate the contributions according to color factors as in [19]. To make the comparison with [19] possible we have given the contribution to the relevant processes also in the notation used in [19]. Using the same definitions of momenta and variables as in [19] the integration of the $2 \rightarrow 3$ matrix elements over the phase space $d\text{PS}^{(r)}$ yields for $P^2 = 0$ the following result ($i = 1, 2, 3, 4$):

$$\int d\text{PS}^{(r)} H_{K_i} = \int_{x_a}^1 \frac{dz_a}{z_a} e^2 g^2 \mu^{4\epsilon} 8(1 - \epsilon) \frac{\alpha_s}{2\pi} \left(\frac{4\pi\mu^2}{s} \right)^\epsilon \frac{\Gamma(1 - \epsilon)}{\Gamma(1 - 2\epsilon)} \frac{1}{4} K_i \quad . \quad (1)$$

Table 1: Classification of $2 \rightarrow 3$ matrix elements

Class	Process	Class in [19]
K_1	$\gamma q \rightarrow qgg$	$I_1 + I_2$
K_2	$\gamma g \rightarrow q\bar{q}g$	$I_6 + I_7$
K_3	$\gamma q \rightarrow qq\bar{q}$	$I_3 + I_4 + I_5$
K_4	$\gamma q \rightarrow qq'\bar{q}'$	I_5

The result for the K_i can easily be read from the results in appendix C of [19] by adding the corresponding sums of I_i 's according to Tab. 1. The result is written in the following form

$$K_1 = 2C_F M U_1(s, t, u) \quad (2)$$

$$K_2 = -2M \left[U_1(t, s, u) + U_1(u, s, t) \right] \quad (3)$$

$$K_3 = 4C_F M \left[U_s(s, t, u) + U_2(t, s, u) + \frac{1}{2}(U_3(s, t, u) + \text{cycl. permutations in } s, t, u) \right] \quad (4)$$

$$K_4 = 2C_F M \left[U_3(s, t, u) + \text{cycl. permutations in } s, t, u \right] \quad (5)$$

where M is defined as

$$M = -\frac{1}{\epsilon} \frac{1}{2N_C} P_{q_i \leftarrow \gamma}(z_a) + \frac{1}{2N_C} P_{q_i \leftarrow \gamma}(z_a) \ln \left(\frac{(1-z_a)}{z_a} y_s \right) + \frac{Q_i^2}{2} \quad (6)$$

In (6) $z_a = \frac{p_1 p_2}{p_0 q} \in [x_a, 1]$ and the splitting function

$$P_{q_i \leftarrow \gamma}(z_a) = 2N_C Q_i^2 \frac{z_a^2 + (1-z_a)^2}{2} \quad (7)$$

The functions $U_i(s, t, u)$ are the LO parton-parton scattering cross sections related to the various processes as shown in Tab. 2. Processes, which are related by crossing are omitted, the complete list is given in [19], q and q' denote quarks with different flavors. The explicit expressions for the U_i and their dependence on color factors are given in [19]. The factor M contains the characteristic singularity proportional to $1/\epsilon$ which is subtracted by absorbing

$$R_{q_i \leftarrow \gamma}(z_a, M_\gamma^2) = -\frac{1}{\epsilon} P_{q_i \leftarrow \gamma}(z_a) \frac{\Gamma(1-\epsilon)}{\Gamma(1-2\epsilon)} \left(\frac{4\pi\mu^2}{M_\gamma^2} \right)^\epsilon \quad (8)$$

into the PDF of the photon $F_{a/\gamma}(x_a, M_\gamma^2)$ (see [19]). This subtraction produces the factorization scale (M_γ) dependence of the photon PDF and gives the finite contributions to the cross section which are given by (2)–(5) with M replaced by $M_{\overline{MS}}$:

$$M_{\overline{MS}} = -\frac{1}{2N_C} P_{q_i \leftarrow \gamma}(z_a) \ln \left(\frac{M_\gamma^2 z_a}{y_s s (1-z_a)} \right) + \frac{Q_i^2}{2} \quad (9)$$

The variable y_s which appears in (6) and (9) is the invariant mass cut-off used to isolate the collinear singularity in the $\gamma \rightarrow q\bar{q}$ splitting.

The procedure for virtual photons with virtuality P^2 is completely analogous. First one calculates the $2 \rightarrow 3$ matrix elements, but now with $P^2 \neq 0$ and decomposes them into terms with the characteristic denominator from $\gamma \rightarrow q\bar{q}$ splitting which become singular

Table 2: LO parton-parton scattering matrix elements

Process	Matrix elements $ \mathcal{M} ^2 = 8N_C C_F g^4 U_i$
$q\bar{q} \rightarrow gg$	$U_1(s, t, u)$
$qq' \rightarrow qq'$	$U_2(s, t, u)$
$qq \rightarrow qq$	$U_2(s, t, u) + U_2(s, u, t) + U_3(s, t, u)$

in the limit $P^2 \rightarrow 0$. These terms after phase space integration up to a cut-off y_s as in (1) have the same structure as (2)–(5) with the LO parton-parton matrix elements factored out. The integration can be done with $\epsilon = 0$ since $P^2 \neq 0$. The phase space in (1) then contains the additional P^2 -dependent factor f

$$f = 1 + \frac{P^2(1 - z_a)}{z_a(z_a s - P^2)} \quad (10)$$

which reduces to 1 for $P^2 = 0$. The factor M in the equations (2)–(5) takes the simple form

$$M = \frac{1}{2N_C} \ln \left(1 + \frac{y_s s}{z_a P^2} \right) P_{q_i \leftarrow \gamma}(z_a) \quad (11)$$

which is singular for $P^2 = 0$ as to be expected. This singularity is absorbed into the PDF of the virtual photon with virtuality P^2 . Instead of (8) the subtraction term is:

$$R_{q_i \leftarrow \gamma}(z_a, M_\gamma^2) = \ln \left(\frac{M_\gamma^2}{P^2(1 - z_a)} \right) P_{q_i \leftarrow \gamma}(z_a) - N_c Q_i^2 \quad . \quad (12)$$

After this subtraction the remaining finite term (for $P^2 \rightarrow 0$) in M yields

$$M(P^2)_{\overline{MS}} = -\frac{1}{2N_c} P_{q_i \leftarrow \gamma}(z_a) \ln \left(\frac{M_\gamma^2 z_a}{(z_a P^2 + y_s s)(1 - z_a)} \right) + \frac{Q_i^2}{2} \quad . \quad (13)$$

In addition to the singular term $\ln(M_\gamma^2/P^2)$ we have subtracted in (12) two finite terms in order to achieve in (13) the same result as in (9) for $P^2 = 0$. Therefore we call this form of factorization the \overline{MS} factorization for $P^2 \neq 0$. It is defined by the requirement that the remaining finite term is equal to the finite term in (2)–(5) with M replaced by $M_{\overline{MS}}$ as was obtained in the calculation for real photons. With this definition of factorization in the case $P^2 \neq 0$ we make sure that we obtain the same NLO corrections as in [19], where $P^2 = 0$, when in the $P^2 \neq 0$ calculation we choose P^2 extremely small. So, for the actual calculations we apply the formulas (2)–(5) where M is now given by (13). We note that for averaging over the spin of initial gluons and photons we apply a factor $1/(2 - 2\epsilon)$, that gives rise to some additional finite terms which should be included in (9) when expanded

in ϵ . We have taken these terms into account also in our calculation. This completes the calculation of the contribution from the photon initial state singularity.

It is clear that in NLO the PDF for the virtual photon must be given also in the $\overline{\text{MS}}$ factorization scheme. In ref. [10] the PDF is constructed in the so-called DIS_γ scheme, which is defined as for real photons ($P^2 = 0$). This distribution function is related to the $\overline{\text{MS}}$ scheme PDF in the following way [10]:

$$F_{a/\gamma}(x, M_\gamma^2)_{\text{DIS}_\gamma} = F_{a/\gamma}(x, M_\gamma^2)_{\overline{\text{MS}}} + \delta F_{a/\gamma}(x, M_\gamma^2) \quad (14)$$

where for $a = q_i, \bar{q}_i$ or g :

$$\begin{aligned} \delta F_{q_i/\gamma}(x, M_\gamma^2) &= \delta F_{\bar{q}_i/\gamma}(x, M_\gamma^2) \\ &= \frac{\alpha}{2\pi} N_C \left[\frac{1}{N_C} P_{q_i \leftarrow \gamma}(x) \ln \left(\frac{1-x}{x} \right) + Q_i^2 8x(1-x) - Q_i^2 \right] \\ \delta F_{g/\gamma}(x, M_\gamma^2) &= 0 \quad . \end{aligned} \quad (15)$$

If the PDF in this scheme is used to calculate the resolved cross section one must transform the NLO finite terms in the direct cross section. This produces a shift of $M(P^2)_{\overline{\text{MS}}}$ as given in (13) by the same expression as (15). Then the relation is:

$$M_{\text{DIS}_\gamma}(P^2) = M(P^2)_{\overline{\text{MS}}} - N_C \left[\frac{1}{N_C} P_{q \leftarrow \gamma}(z_a) \ln \left(\frac{1-z_a}{z_a} \right) + Q_i^2 8z_a(1-z_a) - Q_i^2 \right] \quad . \quad (16)$$

All other singular terms in the real corrections, i.e. final state singularities and the contributions from parton initial state singularities have been calculated by Graudenz in connection with the NLO corrections for jet production in deep inelastic ep scattering. They can be taken from his work [20] together with the virtual corrections up to $\mathcal{O}(\alpha\alpha_s^2)$. (For related work see [21].) All these contributions are calculated in dimensional regularization. The appearing singularities in $1/\epsilon$ cancel when all singular terms are added. The remaining finite terms enter the NLO corrections for the jet cross sections. These finite terms depend on the phase space slicing parameter y_s which is introduced to separate the singular regions of final and initial state infrared and collinear divergences.

3 Inclusive One- and Two-Jet Cross Sections

In this section, we present some characteristic numerical results for one- and two-jet cross sections as a function of the virtuality P^2 . We consider the contributions of the direct and resolved components and their sum. Partly we shall compare the NLO results with LO predictions. The input for our calculation is the following. We have chosen the CTEQ3M proton structure function [22] which is a NLO parametrization with $\overline{\text{MS}}$ factorization and $\Lambda_{\overline{\text{MS}}}^{(4)} = 239$ MeV. This Λ value is also used to calculate α_s from the two-loop formula at the scale $\mu = E_T$. The factorization scales are also $M_\gamma = M_p = E_T$. We also need the parton distribution of the virtual photon $F_{a/\gamma}$. For this we choose either the GRS [12] set or the SaS1M set of Schuler and Sjöstrand [11]. Both sets are given in parametrized form

for all scales M_γ^2 so that they can be applied without repeating the computation of the evolution. Unfortunately both sets are given only in LO, i.e. the boundary conditions for $P^2 = M_\gamma^2$ and the evolution equations are in LO. In [10] PDF's for virtual photons have been constructed in LO and NLO. Distinct differences occur for larger P^2 and $x > 10^{-3}$ which is mainly due to the different NLO perturbative boundary condition at $P^2 = M_\gamma^2$, which does not exist for the real ($P^2 = 0$) photon structure function. Since neither of the two PDF's is constrained by empirical data from scattering on a virtual photon target we consider these LO distribution functions as sufficient for our exploratory studies on jet production and treat them as if they were obtained in NLO. In particular, we shall use the transformation formulae (14) for going from the DIS_γ to the $\overline{\text{MS}}$ -scheme PDF, which makes sense only in NLO. Then the parametrization [12] is considered as the parametrization in the DIS_γ scheme. In the PDF of GRS the input scale is $Q_0 = 0.5$ GeV and the restriction $P^2 \leq Q^2/5$ is implemented as to fulfill the condition $\Lambda^2 \ll P^2 \ll Q^2$. In addition the PDF of GRS is constructed only for $N_f = 3$ flavors. The production of the heavier c and b quarks is supposed to be added as predicted by perturbation theory of fixed order with no active c and b quarks in the proton and photon PDF's. In LO this amounts to adding the processes $\gamma^* g \rightarrow c\bar{c}$ and $\gamma^* g \rightarrow b\bar{b}$ to the cross section, keeping $m_c, m_b \neq 0$. Since in this work we are primarily interested in studying the sum of the direct and resolved contributions and the influence of the consistent subtractions of the NLO direct part we refrain from adding the LO or NLO cross sections for direct heavy quark production as suggested in [10, 12]. So, our investigations in connection with the GRS parametrization of the virtual photon PDF are for a model with three flavors only. For consistency we take also $N_f = 3$ in the NLO corrections and in the two-loop formula for α_s . To overcome this problem we studied the relevant cross sections also with the virtual photon PDF's of [11]. Here the c quark is included as a massless flavor in the PDF which undergoes the usual evolution as the other massless quarks except for a shift of the starting scale Q_0 . This $N_f = 4$ PDF is considered only in the parametrization SaS1M with $Q_0 = 0.6$ GeV that is in the $\overline{\text{MS}}$ scheme.

The cross sections we have computed are essentially for kinematical conditions as in the HERA experiments. There, positrons of $E_e = 27.5$ GeV produce photons with virtuality P^2 which then collide with a proton of $E_p = 820$ GeV. The momentum transfer to the photon is $q = p_e - p'_e$ with $P^2 = (-q^2)$. The energy spectrum of the virtual photons is approximated by

$$\frac{dF_{\gamma/e}(y)}{dP^2} = \frac{\alpha}{2\pi} \frac{1 + (1-y)^2}{y} \frac{1}{P^2} \quad (17)$$

with

$$y = \frac{pq}{pp_e} \simeq \frac{E_{\gamma^*}}{E_e} \quad (18)$$

being the fraction of the electron energy transferred to the photon, when the virtuality $P^2 \ll E_{\gamma^*}^2$. The momentum of the incoming proton is p . The approximation for the virtual photon spectrum is used for the calculation of the resolved and the direct cross section. The expression (17) factorizes in the cross section for $ep \rightarrow e'X$ with arbitrary final state X if one neglects the longitudinal virtual photon terms. After integration over P^2 between

$P_{min}^2 < P^2 < P_{max}^2$ with $P_{min}^2 := m_e^2 y^2 / (1 - y)$, where m_e is the electron mass, one obtains the Weizsäcker-Williams formula as used for calculations with untagged electrons as in [4, 19], where $P^2 \simeq 0$ dominates. The cross section for the process $ep \rightarrow e'X$ is then given by the convolution

$$\frac{d\sigma(ep \rightarrow e'X)}{dP^2} = \int_{y_{min}}^{y_{max}} dy \frac{dF_{\gamma/e}(y)}{dP^2} d\sigma(\gamma^*p \rightarrow X) \quad (19)$$

where $d\sigma(\gamma^*p \rightarrow X)$ denotes the cross section for $\gamma^*p \rightarrow X$ with transversely polarized photons of energy $q_0 = E_e y - P^2 / (4E_e y)$, if the transverse component of q is neglected. To have the equivalent conditions as in the ZEUS analysis we choose $y_{min} = 0.2$ and $y_{max} = 0.8$. In the computation of the resolved cross section the approximation $q_0 = E_e y$ is inserted for the energy of the virtual photon, whereas for the direct photon cross section the exact relation for q_0 is taken into account through the kinematic relations.

All further calculations proceed in the following way. For both, the direct and the resolved cross section, we have a set of two-body contributions and a set of three-body contributions. Each set is completely finite, as all singularities have been canceled or absorbed into PDF's. Each part depends separately on the phase space slicing parameter y_s . The analytic calculations are valid only for very small y_s , since terms $\mathcal{O}(y_s)$ have been neglected in the analytic integrations. For very small y_s , the two separate pieces have no physical meaning. In this case the $(\ln y_s)$ -terms force the two-body contributions to become negative, whereas the three-body cross sections are large and positive. In [3] we have plotted such a cross sections for direct real photoproduction at $y_s = 10^{-3}$. When the two-body and three-body contributions are superimposed to yield a suitable inclusive cross section, as for example the inclusive one- or two-jet cross section, the dependence on the cut-off y_s will cancel. The separation of the two contributions with the slicing parameter y_s is a purely technical device in order to distinguish the phase space regions, where the integrations are done analytically, from those, where they are done numerically. We have checked, by varying y_s between 10^{-4} and 10^{-3} , that the superimposed two- and three-body contributions are independent of y_s for the inclusive single- and dijet cross sections.

First, we study the inclusive single-jet cross section. To calculate it we must choose a jet definition, which combines two nearly collinear partons. We adopt the jet definition of the Snowmass meeting [23]. According to this definition, two partons i and j are recombined, if $R_{i,j} < R$, where $R_{i,j} = \sqrt{(\eta_i - \eta_j)^2 + (\phi_i - \phi_j)^2}$ and η_j, ϕ_j are the rapidity and the azimuthal angle of the combined jet respectively, defined as

$$E_{T_J} = E_{T_1} + E_{T_2} \quad (20)$$

$$\eta_J = \frac{E_{T_1} \eta_1 + E_{T_2} \eta_2}{E_{T_J}} \quad , \quad (21)$$

$$\phi_J = \frac{E_{T_1} \phi_1 + E_{T_2} \phi_2}{E_{T_J}} \quad , \quad (22)$$

and R is chosen as in the experimental analysis. So, two partons are considered as two separate jets or as a single jet depending whether they lie outside or inside the cone with

radius R around the jet momentum. In NLO, the final state may consist of two or three jets. The three-jet sample contains all three-body contributions, which do not fulfill the cone condition. The cone constraint is evaluated in the HERA laboratory system as for real photoproduction ($P^2 = 0$) and in the experimental analysis. The calculation of the resolved cross section proceeds as for real photoproduction, i.e. the transverse momentum (q_T) of the virtual photon is neglected so that the virtual photon momentum is in the direction of the incoming electron and $q_0 = E_e y$. The cross section for direct photons, in which the initial state singularity is subtracted, as specified in the previous section, is given in the center-of-mass system $\mathbf{p} + \mathbf{q} = \mathbf{0}$ and transformed into the HERA laboratory system, again neglecting q_T and other small terms proportional to P^2 . Then the relation between the rapidity η_{cm} of the jet in the c.m.-system and laboratory system is as for real photoproduction, which is

$$\eta = \eta_{cm} + \frac{1}{2} \ln \frac{E_p}{y E_e} \quad . \quad (23)$$

This η and the corresponding azimuthal angle of the partons in the final state is also used for evaluating the jet definition given above.

In Fig. 1a, b, c, the results for $d^3\sigma/dE_T d\eta dP^2$ are shown integrated over η in the interval $-1.125 \leq \eta \leq 1.875$ (these boundaries are employed in the ZEUS analysis [15]) as a function of E_T for the three values of $P^2 = 0.058, 0.5$ and 1 GeV^2 . The smallest value of P^2 has been chosen in such a way that it reproduces the $P^2 \simeq 0$ results. Inserting $P^2 = 0.058 \text{ GeV}^2$ into the unintegrated Weizsäcker-Williams formula corresponds to the one integrated in the region $P_{min}^2 \leq P^2 \leq P_{max}^2 = 4 \text{ GeV}^2$. For all three P^2 the cross section is dominated by the resolved component at small E_T . Near $E_T = 20 \text{ GeV}$ the direct component, which is the direct cross section without the subtraction term, denoted by Dir_s , is of the same magnitude as the resolved cross section. As a function of P^2 the cross section $d^3\sigma/dE_T d\eta dP^2$ decreases more or less uniformly in the considered E_T range with increasing P^2 . One can see that this decrease is stronger for small E_T as compared to large E_T . In these and the following results the cone radius is $R = 1$. The corresponding rapidity distribution for a fixed E_T will be shown later in Fig. 5a, b, c, d for the SaS1M photon PDF.

In Fig. 2a, b, c we studied the η distribution of the Dir_s contribution at fixed $E_T = 7 \text{ GeV}$ and the same P^2 values as in Fig. 1 in comparison with two approximations, namely the LO cross section and the NLO cross section with $P^2 \neq 0$ only in the photon flux equation (17) and the rest of the cross section evaluated at $P^2 = 0$ as in [19]. As to be expected this approximation is very good for $P^2 = 0.058 \text{ GeV}^2$. At the larger P^2 however it overestimates the cross section and should not be used. This means that the P^2 dependence of the direct part, although the strongest logarithmic P^2 dependence has been subtracted, should be taken into account. Of course, in the sum of the resolved and the direct cross section the difference is small as long as the resolved part dominates which is true for the smaller E_T 's. The LO prediction, which is evaluated with the same structure functions and α_s value as the NLO result, only the hard scattering cross section is calculated in LO, is smaller than the NLO result, the difference decreasing with increasing P^2 . Of course, this finding depends on the chosen value of R . The NLO cross section

depends on R , whereas the LO curve does not. Therefore estimates of the inclusive cross section with LO calculations can be trusted only for large cone radii.

It is clear that the resolved and the direct cross sections decrease with increasing P^2 for fixed η and E_T . It is of interest to know how the ratio of resolved and the direct cross section behaves as a function of P^2 . This is a well defined quantity in LO. The variation of this ratio with P^2 up to $P^2 = 4 \text{ GeV}^2$ for $E_T = 7 \text{ GeV}$ and $\eta = 2, 1, 0$ and -1 is plotted in Fig. 3a, b, c, d. As we expected this ratio decreases most strongly for $\eta = 2$, since in the $\eta > 0$ region the resolved component dominates whereas the direct cross section peaks for negative η 's (see Fig. 2a, b, c). If we decrease η towards the backward direction this ratio diminishes more or less uniformly for all P^2 . In NLO this ratio depends on the scheme chosen for the photon PDF. In the DIS_γ subtraction scheme terms in the photon PDF are shifted to the direct cross section as follows from (14)–(16) in section 2. This necessarily changes the ratio of the resolved to the direct cross section, not only in the absolute value but also in the dependence on P^2 . For all η 's this ratio is quite different from its LO value. The difference between the $\overline{\text{MS}}$ and DIS_γ scheme is small for $\eta = 0, 1$ moderate for $\eta = 2$ and of the order of 1.5 at $\eta = -1$. Except at $\eta = -1$ the ratio is always larger in the DIS_γ scheme than in the $\overline{\text{MS}}$ scheme. Apart from the fact that the ratios plotted in Fig. 3a, b, c, d cannot be measured directly, they are scheme dependent in NLO and have very large corrections when going from LO to NLO. In Fig. 3a, b, c we have also plotted the ratio for the case that the P^2 dependence is neglected in the cross section $\gamma^*p \rightarrow X$ and taken into account only in the photon propagator (denoted $\text{NLO}(P^2 = 0)$). This approximation gives a result very similar to the LO curve showing that the NLO corrections are more important for $P^2 \neq 0$. Of course at $P^2 \rightarrow 0$ this approximation is equal to the NLO result in the $\overline{\text{MS}}$ scheme.

The results shown so far are for a model with three flavors only and therefore should not be compared to the experimental data except when the contribution from the charm quark is added at least in LO. A more realistic approach is to use the photon PDF's SaS1M of ref. [11] which are constructed for four flavors. The results for $d^3\sigma/dE_T d\eta dP^2$ integrated over $\eta \in [-1.125, 1.875]$ as a function of E_T for $P^2 = 0.058, 0.5$ and 1.0 GeV^2 are presented in Fig. 4a, b, c. These curves can be compared with the results in Fig. 1a, b, c obtained with the GRS photon distribution with $N_f = 3$. The results for the sum of the resolved and direct contributions change between 10% and 30% in the small E_T region and approximately 50% in the large E_T region. As one can see the larger cross section for $N_f = 4$ results primarily from the direct component. Since the direct component is more important for large E_T than for small E_T the increase is stronger in the former region.

Of interest are also the rapidity distributions for fixed E_T . These are shown for $E_T = 7 \text{ GeV}$ as a function of η between $-1 \leq \eta \leq 2$ choosing $P^2 = 0.058, 1, 5$ and 9 GeV^2 in Fig. 5a, b, c, d. We show the subtracted direct cross section and the resolved cross section and their sum for the photon PDF as in Fig. 4a, b, c. Expectedly the resolved component has its maximum shifted to positive η 's as compared to the direct component. The direct component falls off with increasing η quite strongly. This comes from the subtraction of the $(\ln P^2)$ terms as is apparent when we compare with the unsubtracted direct cross section, labeled "Dir" in Fig. 5a, b, c, d. The sum of the resolved and the

direct (subtracted) cross section is more or less constant for the smaller P^2 values and decreases with increasing η for $P^2 = 5$ and 9 GeV^2 .

For large enough P^2 we expect the unsubtracted direct cross section to be the correct one. In this region the subtraction term (12) must approximate the PDF of the photon rather well. We have checked this by a direct comparison. With increasing P^2 the full direct cross section (Dir) approaches the Sum=Res+Dir_s better and better. But even at $P^2 = 9 \text{ GeV}^2$ the two cross sections differ at $\eta = 2$ still by approximately 30 %. However, in the backward direction at $\eta = -1$ we also see a difference. In this region, which corresponds in the photon PDF to the region $x_\gamma \simeq 1$, where the perturbative component dominates, we do not expect a deviation. This may be caused by our approximation of neglecting the transverse momentum q_T of the virtual photon in the relation (22) and in the calculation of the resolved cross section.

In order to compare with preliminary data for the dijet cross section presented by the ZEUS collaboration [15] we calculated the inclusive dijet cross section $d^4\sigma/dE_T d\eta_1 d\eta_2 dP^2$ as a function of P^2 . Here E_T is the transverse energy of the measured or trigger jet with rapidity η_1 . η_2 denotes the rapidity of another jet such that in the three-jet sample these two jets have the largest E_T , i.e. $E_{T_1}, E_{T_2} > E_{T_3}$. The calculational procedure is analogous to the inclusive single-jet cross section and follows closely the work presented in [4] for $P^2 = 0$. Since inclusive two-jet cross sections depend on one more variable they constitute a much more stringent test of QCD predictions than inclusive one-jet cross sections. We could predict distributions in η_1 and η_2 for fixed E_T or distributions in E_T for various values of the two rapidities η_1 and η_2 in the same way as in [4] for $P^2 = 0$. Since no such information is expected from the experiment in the near future we calculated only the E_T distribution with the two rapidities integrated over the interval $-1.125 < \eta_1, \eta_2 < 1.875$ following the constraints in the ZEUS analysis [15]. The results for $P^2 = 0.058, 0.5$ and 1.0 GeV^2 are shown in Fig. 6a, b, c, where the full curve is $d^4\sigma/dE_T d\eta_1 d\eta_2 dP^2$ as a function of E_T integrated over η_1 and η_2 in the specified interval and for $0.2 < y < 0.8$. The functional dependence on E_T does not change as a function of P^2 , only the absolute value of the cross section decreases with increasing P^2 .

In Fig. 6a, b, c we show also the cross sections for enriched direct and resolved γ samples. These cross sections are labeled "Dir" (dashed curve) and "Res" (dotted curve), respectively. The two cross sections are defined with a cut on the variable x_γ^{obs} where x_γ^{obs} is defined by

$$x_\gamma^{obs} = \frac{\sum_i E_{T_i} e^{-\eta_i}}{2yE_e} \quad . \quad (24)$$

This variable measures the fraction of the proton energy that goes into the production of the two hardest jets. The "Dir" curve gives the cross section for $x_\gamma^{obs} > 0.75$. This cut on x_γ^{obs} leads to an enrichment of the direct component of the cross section, since exclusive two-jet events from the direct process have $x_\gamma^{obs} = 1$. The curve labeled "Res" gives the cross section in the complementary region $x_\gamma^{obs} < 0.75$ which characterizes the enriched resolved γ sample. The sum of the Dir and Res curves is equal to the full cross section $d^4\sigma/dE_T d\eta_1 d\eta_2 dP^2$ with no cut on x_γ^{obs} . It must be emphasized that both cross sections, whether $x_\gamma^{obs} > 0.75$ or $x_\gamma^{obs} < 0.75$, contain contributions from the direct and resolved

part. Actually the resolved contribution in the enriched direct sample ($x_\gamma^{obs} > 0.75$) is non-negligible. The results in Fig. 6a, b, c are for the GRS parton distributions in the $\overline{\text{MS}}$ scheme. As to be expected, with increasing P^2 the full cross section is more and more dominated by the Dir component, in particular at the larger E_T . This means that the cross section in $x_\gamma^{obs} < 0.75$ decreases stronger with P^2 than in the $x_\gamma^{obs} > 0.75$ region. This could be studied experimentally by measuring the ratio of the two cross sections as a function of P^2 for fixed E_T . This has not been done yet. Instead, the ZEUS collaboration [15] measured the ratio $r = \text{Res}/\text{Dir}$, where Res and Dir are the cross sections as defined above, but integrated over $E_{T_1}, E_{T_2} \geq 4$ GeV. With this integration cut on the transverse momenta of the two hardest jets, the transverse momentum of the third jet may vanish which affords particular constraints on the remnant jets. This is treated as in [3]. Furthermore we replaced the GRS photon PDF by the SaS1M photon PDF which is for $N_f = 4$ flavors. With these assumptions we calculated the ratio r as a function of P^2 up to $P^2 = 0.6$ GeV² and compared it with the ZEUS [15] data in Fig. 7 in LO (dotted curve) and NLO (full curve). The theoretical NLO curve agrees quite well with the data at $P^2 \geq 0.25$ GeV² but not with the measured point at $P^2 \simeq 0.2$ GeV² and at $P^2 = 0.058$ GeV² corresponding to the photoproduction case. Of course the ratio r for $P^2 \simeq 0$ is much more precise and lies 30 % higher than the predicted cross section. This disagreement at $P^2 \simeq 0$ is to be expected since at this value of P^2 the measured inclusive dijet cross section for the enriched resolved γ sample is larger than the predicted cross section for a small E_T cut [4]. As in [4] we attribute this difference between theory and experimental data to additional contributions due to multiple interactions with the proton remnant jet in the resolved cross section not accounted for by our NLO predictions. This underlying event contribution is reduced with increasing E_T^{min} and/or smaller cone radii $R < 1$. As it seems, for larger P^2 , the underlying event contribution is also reduced. Of course this could be studied more directly by measuring rapidity distributions for the enriched resolved γ sample as was done at $P^2 \simeq 0$ in [4].

4 Conclusions

We have calculated inclusive single jet and dijet cross sections for photoproduction with virtual photons. The direct and resolved contributions were calculated in next-to-leading order QCD using the phase-space slicing method. They were folded with the unintegrated Weizsäcker-Williams approximation and existing LO parametrizations for the virtual photon parton densities. The collinear singularity in the direct photon initial state was integrated analytically up to an invariant mass cut-off y_s . Contrary to real photons, this specific singularity is not regulated in the dimensional regularization scheme but by the mass of the virtual photon P^2 leading to a logarithmic dependence on P^2 . This logarithmic term is absorbed into the virtual photon structure function rendering the latter scheme and scale dependent. The remaining finite contribution is constructed in such a way that the corresponding real photon term is obtained in the limit $P^2 = 0$ in the $\overline{\text{MS}}$ scheme. Similarly to the construction of virtual photon structure functions by GRS

and SaS, our calculation of the hard scattering cross section then provides a consistent extension from $P^2 = 0$ to small, but non-zero P^2 .

We presented y_s -cut independent results using the Snowmass jet definition and HERA conditions for distributions in the transverse energy and the rapidity of the observed jet and in the photon virtuality. For the case of very small P^2 , we found good numerical agreement with the predictions for real photoproduction. At $P^2 = 9 \text{ GeV}^2$, the unsubtracted direct contribution corresponding to the case of deep inelastic scattering approximates the sum of the subtracted direct and resolved contributions quite well. A small discrepancy remains in the forward region, where the resolved contribution is dominant. As in the case of $P^2 = 0$, the resolved component dominates at low E_T and in the forward region. The NLO effects were demonstrated to be important in the ratio of resolved and direct cross sections as a function of P^2 . Since the theoretical separation between direct and resolved is artificial, some scheme dependence remains here unless both contributions are defined by an experimental cut on x_γ^{obs} in dijet cross sections. Then the corresponding ratio shows significant NLO effects and good agreement with the available ZEUS data for $P^2 > 0.2 \text{ GeV}^2$. The disagreement below this value can be attributed to additional contributions coming from, e.g., multiple scattering between the photon and proton remnants.

Future investigations on virtual photoproduction will require more data on single inclusive jet production as they exist for $P^2 = 0$ and at larger transverse energies. With luminosity permitting, a detailed dijet analysis of an infrared safe cross section such as $d^4\sigma/dE_T d\eta_1 d\eta_2 dP^2$, where the transverse energies of the two jets are not cut at exactly the same value, will provide a much improved insight into the structure of the virtual photon. Furthermore, choosing a k_T -cluster-like jet definition with smaller cone radii will reduce both the uncertainties in the jet algorithm and in the underlying event. On the theoretical side, one possible improvement is the correct treatment of the transverse momentum of the incoming photon for larger P^2 including a correct transformation from the photonic c.m. frame to the HERA laboratory system. For a consistent NLO treatment, the inclusion of NLO parton densities for the photon is necessary. These are, however, needed in a parametrized form and should also be studied in correlation with deep inelastic $e\gamma^*$ scattering data.

References

- [1] M. Derrick et al., ZEUS Collaboration, Phys. Lett. B322 (1994) 287.
- [2] M. Derrick et al., ZEUS Collaboration, Phys. Lett. B348 (1995) 665.
- [3] M. Klasen, G. Kramer, Phys. Lett. B366 (1996) 385.
- [4] M. Klasen, G. Kramer, DESY 96-246, November 1996, to be published in Z. Phys. C; M. Klasen, DESY 96-204, September 1996.
- [5] ZEUS Collaboration, Contribution to the XXVIII ICHEP, Warsaw, July 1996, pa02-040.

- [6] M. Glück, E. Reya, A. Vogt, Phys. Rev. D46 (1992) 1973; L.E. Gordon, J.K. Storrow, Z. Phys. C56 (1992) 307; P. Aurenche, M. Fontannaz, J.-Ph. Guillet, Z. Phys. C64 (1994) 621.
- [7] For reviews see: A. Vogt, Proceedings of the Workshop on Two-Photon Physics at LEP and HERA, Lund, May 1994, eds. G. Jarlskog and L. Jönssen (Lund Univ., 1994) p. 141; T. Sjöstrand, J.K. Storrow, A. Vogt, J. Phys. G22 (1996) 893.
- [8] Ch. Berger et al., PLUTO Collaboration, Phys. Lett. B142 (1984) 119.
- [9] Report on " $\gamma\gamma$ Physics", conveners P. Aurenche and G.A. Schuler, to appear in the proceedings of the 1995 LEP2 Physics workshop, hep-ph/9601317.
- [10] M. Glück, E. Reya, M. Stratmann, Phys. Rev. D51 (1995) 3220.
- [11] G.A. Schuler, T. Sjöstrand, Z. Phys. C68 (1995) 607, Phys. Lett. B376 (1996) 193.
- [12] M. Glück, E. Reya, M. Stratmann, Phys. Rev. D54 (1996) 5515.
- [13] D. de Florian, C. Garcia Canal, R. Sassot, preprint CERN-TH/96-234, August 1996, to be published in Z. Phys. C, hep-ph/9608438.
- [14] J. Chyla, J. Cvach, Proceedings of the Workshop 1995/96 on "Future Physics at HERA", eds. G. Ingelman, A. de Roeck, R. Klanner, DESY 1996, Vol. 1, p. 545.
- [15] M.L. Utley on behalf of the ZEUS collaboration, Univ. Glasgow report GLAS-PPE/95-03, talk given at EPS Conference, Brussels, 1995, hep-ex/9508016; C. Foudas, ZEUS collaboration, talk given at DIS96 Workshop, Rome, 1996.
- [16] T. Ebert, H1 Collaboration, talk given at DIS96 Workshop, Rome, 1996.
- [17] D. Bödeker, Phys. Lett. B292 (1992) 164, Z. Phys. C59 (1993) 501.
- [18] D. Bödeker, G. Kramer, S.G. Salesch, Z. Phys. C63 (1994) 471; M. Klasen, DESY 96-204, September 1996.
- [19] M. Klasen, G. Kramer, Z. Phys. C72 (1996) 107.
- [20] D. Graudenz, Phys. Rev. D49 (1994) 3291, Phys. Lett. B256 (1992) 518, report DESY-T-90-01, September 1990, unpublished.
- [21] T. Brodtkorb, E. Mirkes, Z. Phys. C66 (1995) 141.
- [22] H.L. Lai et al., CTEQ Collaboration, Phys. Rev. D51 (1995) 4763.
- [23] J.E. Huth et al., Proc. of the 1990 DPF Summer Study on High Energy Physics, Snowmass, Colorado, edited by E.L. Berger, World Scientific, Singapore, 1992, p. 134.

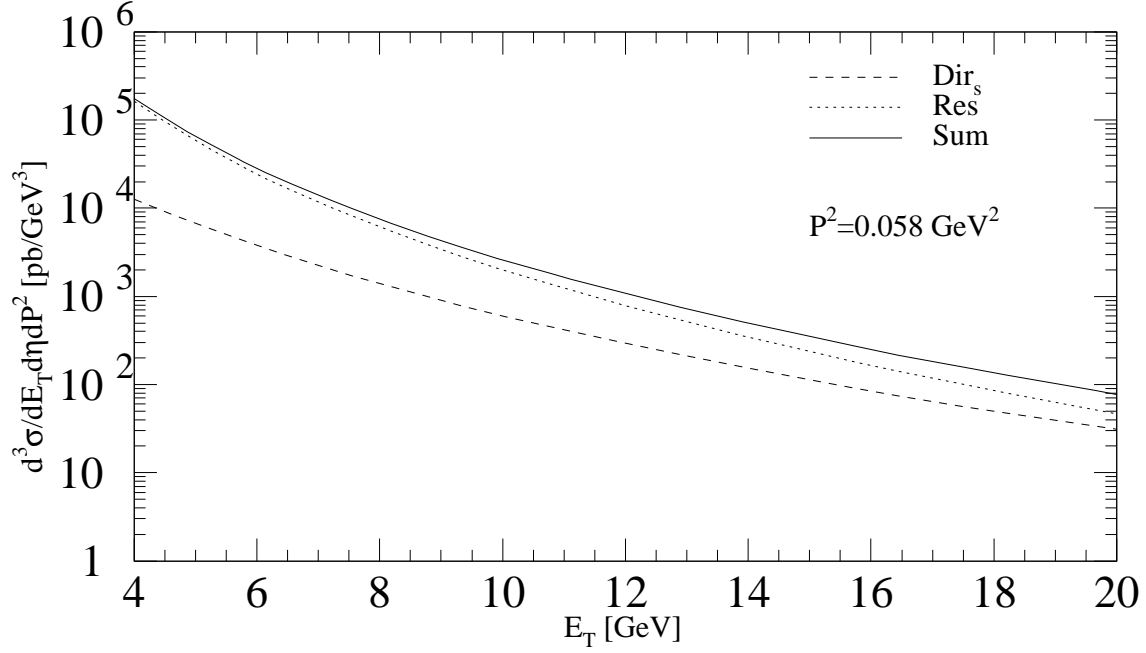


Figure 1a: Single-jet inclusive cross section integrated over $\eta \in [-1.125, 1.875]$ for the virtuality $P^2 = 0.058 \text{ GeV}^2$. The $\overline{\text{MS}}$ -GRS parametrization with $N_f = 3$ is chosen. The solid line gives the sum of the subtracted direct and the resolved term.

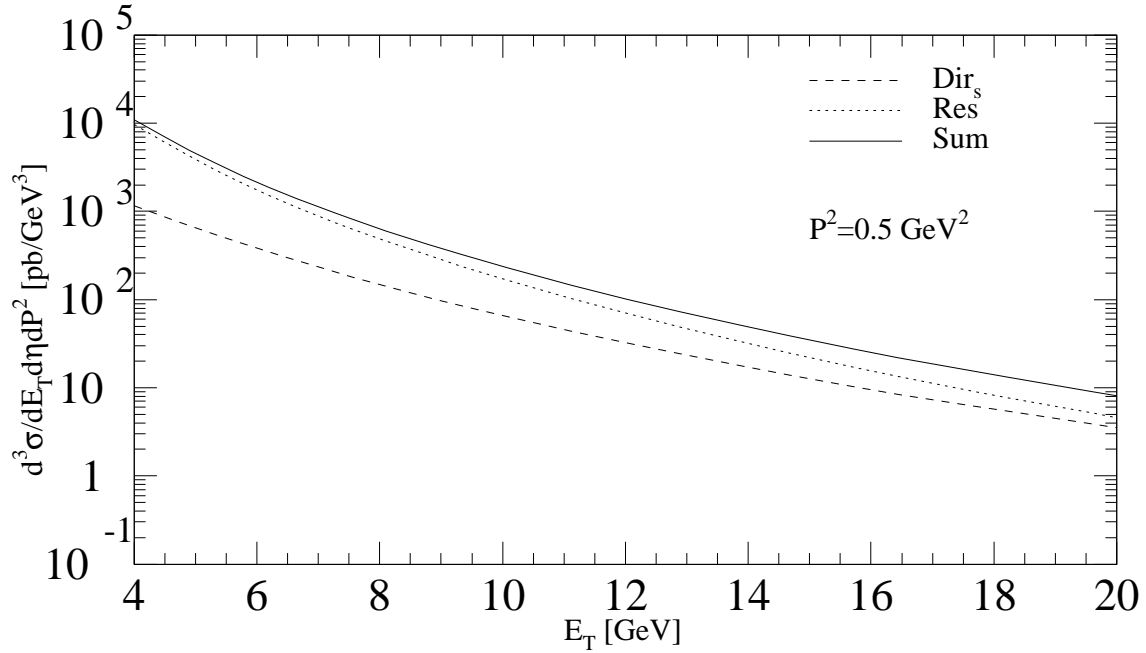


Figure 1b: Same as figure 1a with $P^2 = 0.5 \text{ GeV}^2$.

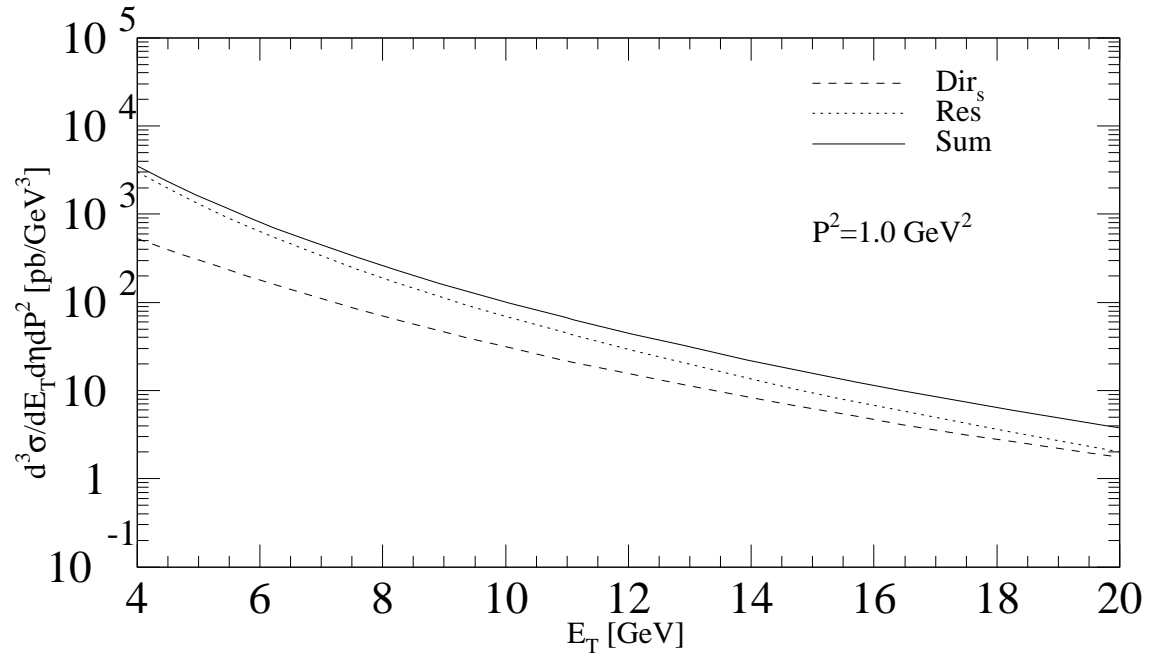


Figure 1c: Same as figure 1a with $P^2 = 1.0 \text{ GeV}^2$.

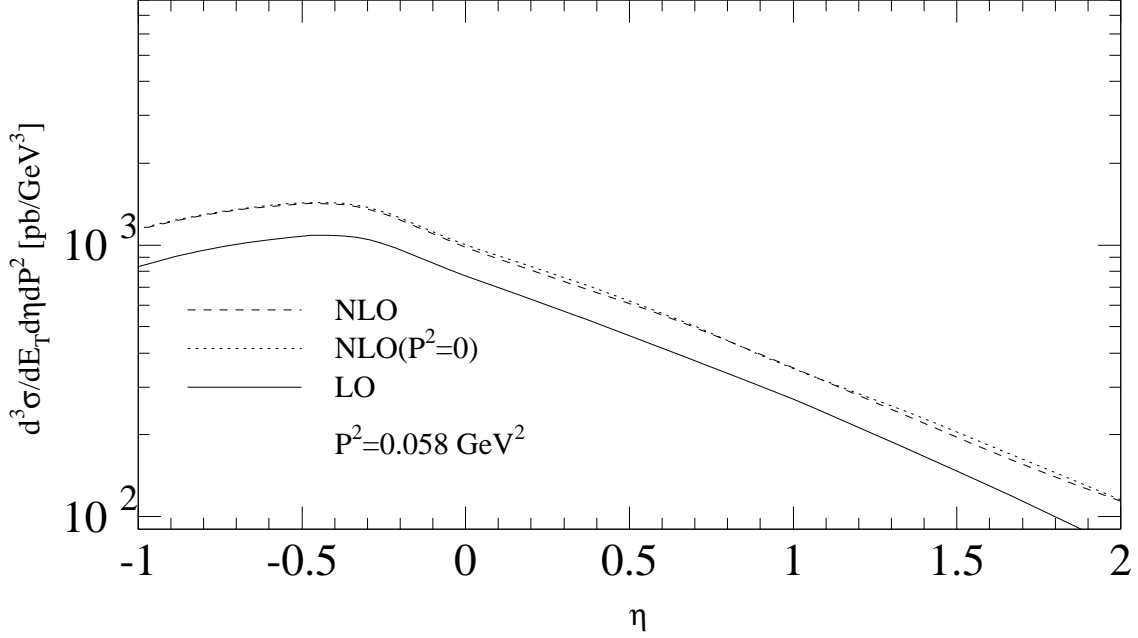


Figure 2a: Single-jet inclusive cross sections for $E_T = 7$ GeV and $P^2 = 0.058$ GeV². The $\overline{\text{MS}}$ -GRS parametrization with $N_f = 3$ is chosen. Only the direct part with subtraction (Dir_s) is plotted. The solid line gives the LO contribution. The dashed curve is the full NLO cross section, whereas the dotted curve gives the NLO cross section, where the NLO matrix elements have no P^2 -dependence.

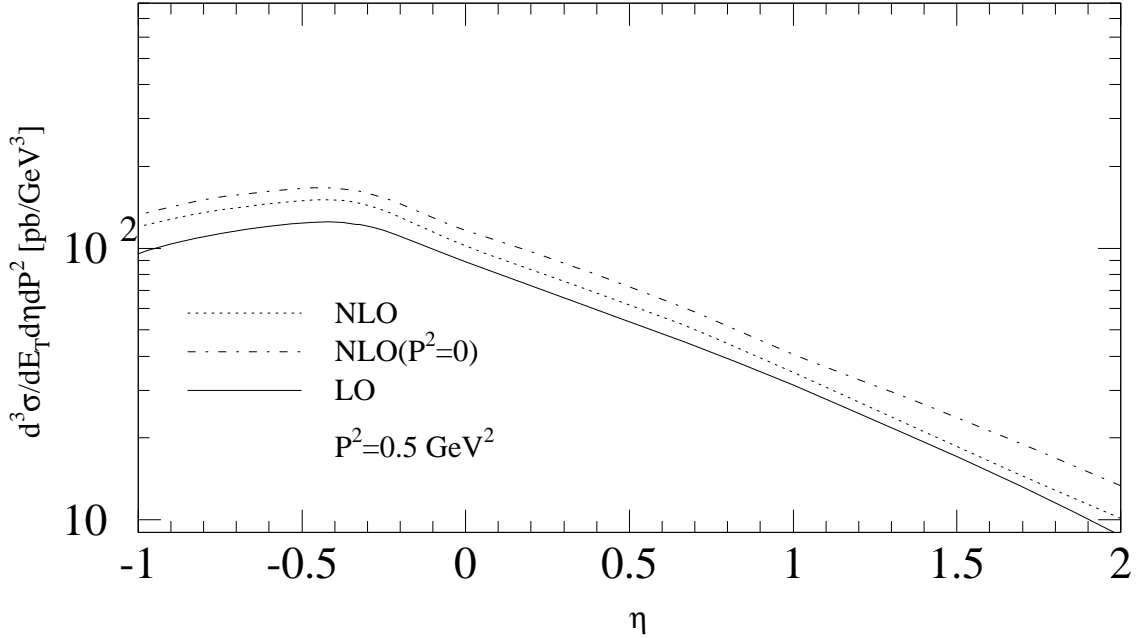


Figure 2b: Same as figure 2a with $P^2 = 0.5$ GeV².

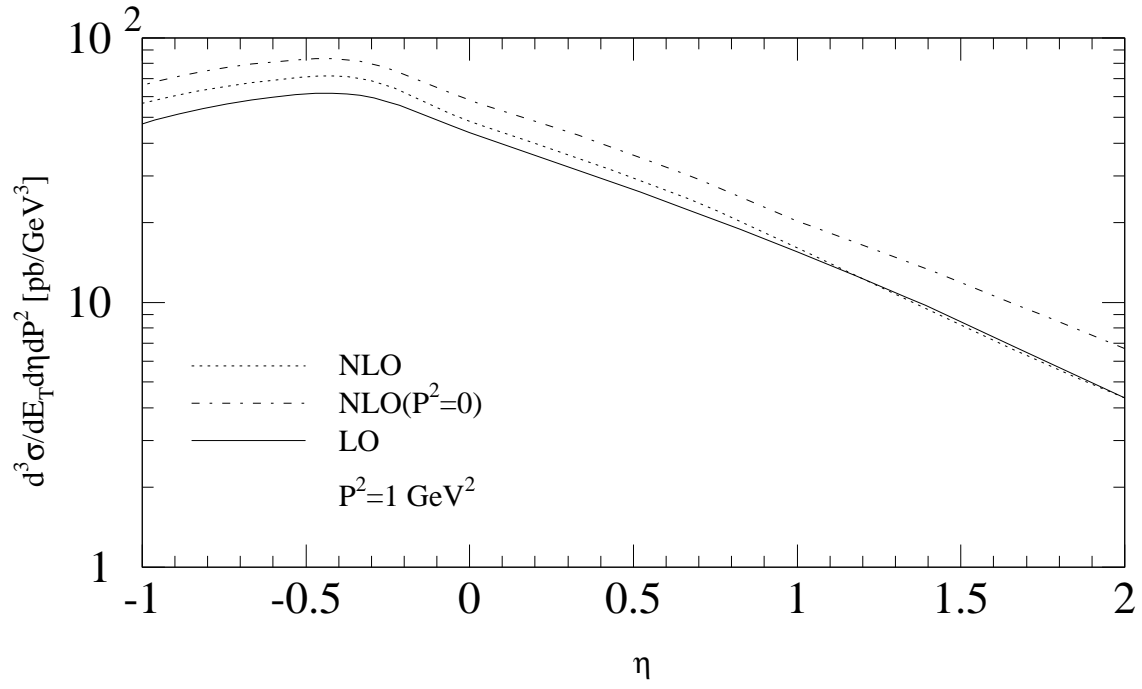


Figure 2c: Same as figure 2a with $P^2 = 1.0 \text{ GeV}^2$.

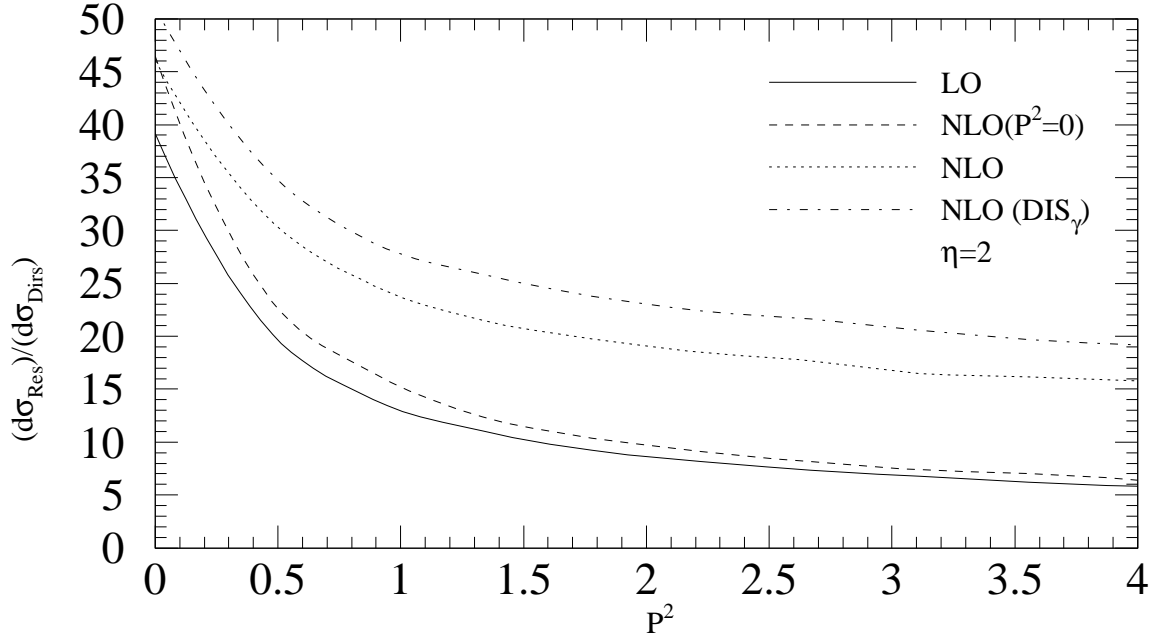


Figure 3a: The ratio of the resolved to the subtracted direct contribution in LO and NLO for the GRS parametrization, both in the $\overline{\text{MS}}$ - and the DIS_γ -scheme for $\eta = 2$ and $E_T = 7$ GeV. The dashed curve is for the NLO-matrix elements with $P^2 = 0$ for comparison.

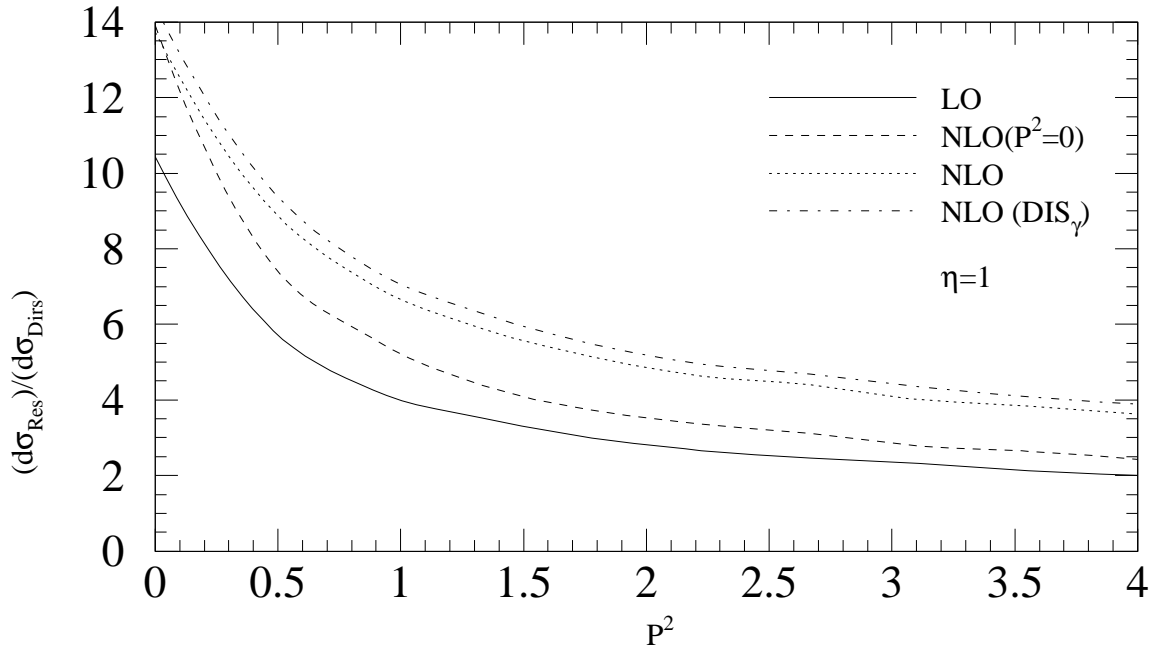


Figure 3b: Same as figure 3a with $\eta = 1$.

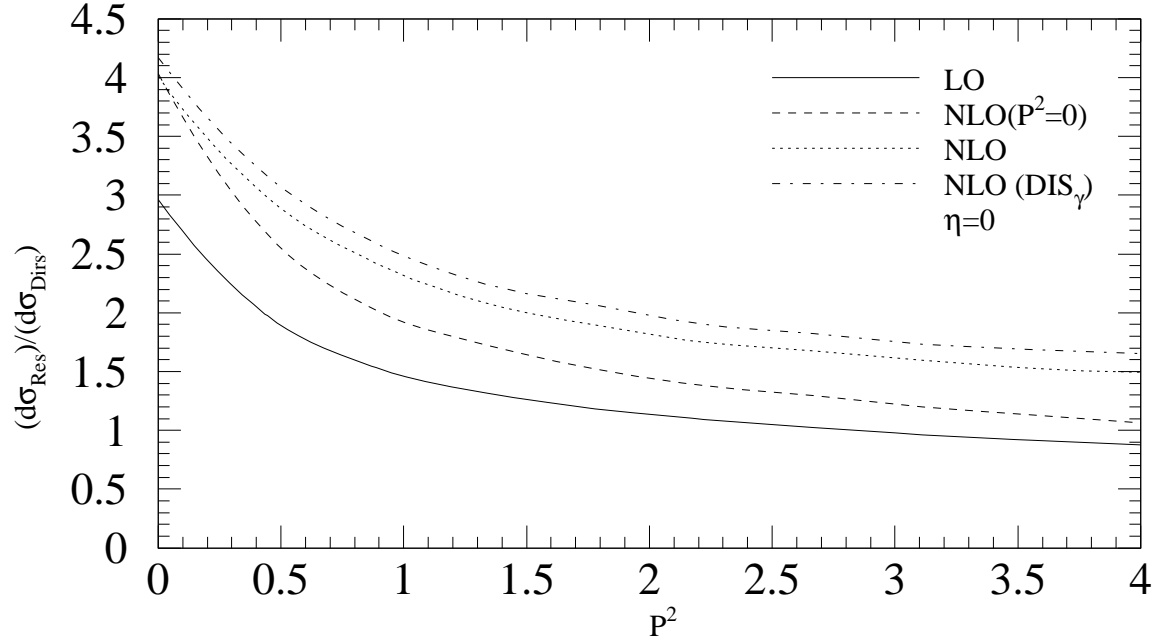


Figure 3c: Same as figure 3a with $\eta = 0$.

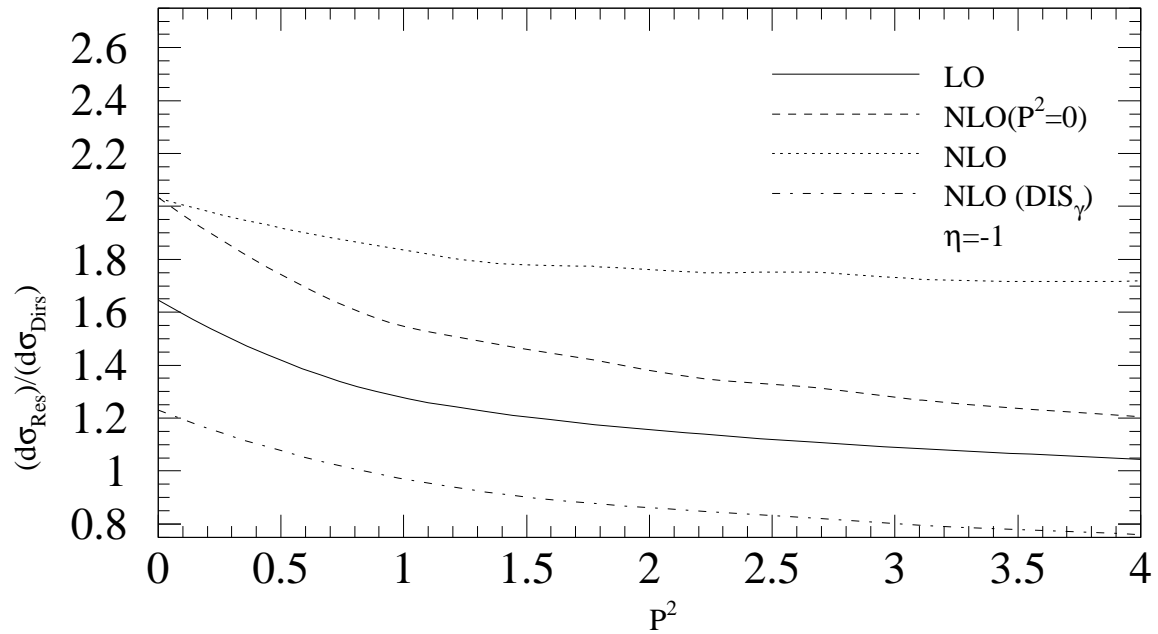


Figure 3d: Same as figure 3a with $\eta = -1$.

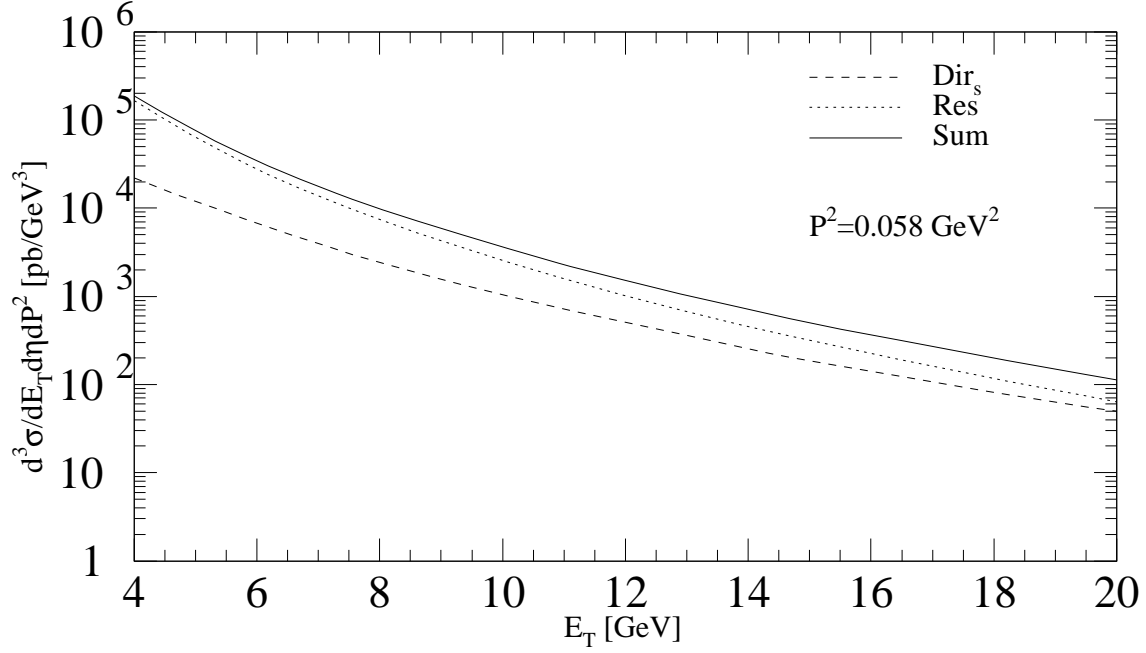


Figure 4a: Single-jet inclusive cross section integrated over $\eta \in [-1.125, 1.875]$ for the virtuality $P^2 = 0.058 \text{ GeV}^2$. The $\overline{\text{MS}}$ -SaS1M parametrization with $N_f = 4$ is chosen. The solid line gives the sum of the subtracted direct and the resolved term.

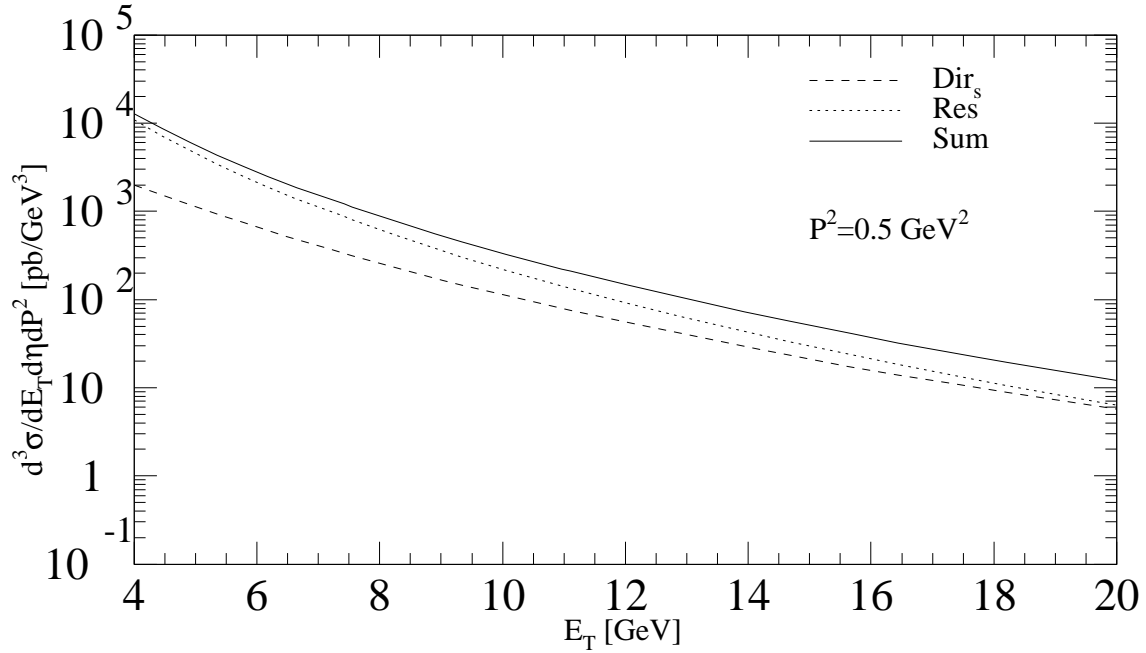


Figure 4b: Same as figure 4a with $P^2 = 0.5 \text{ GeV}^2$.

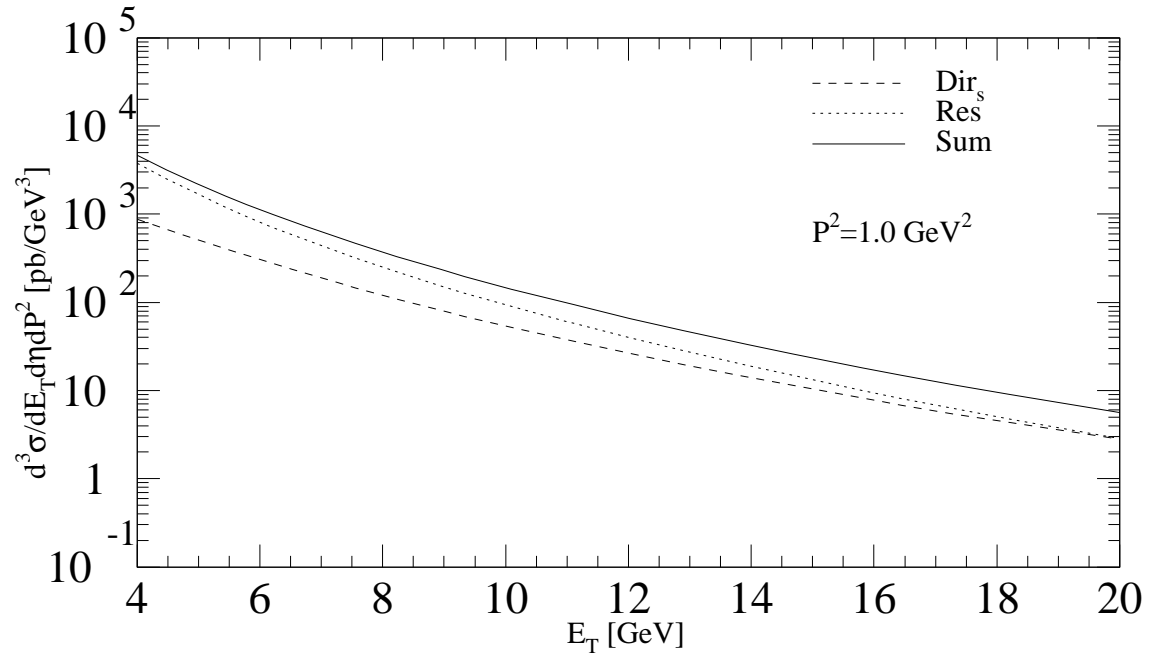


Figure 4c: Same as figure 4a with $P^2 = 1.0 \text{ GeV}^2$.

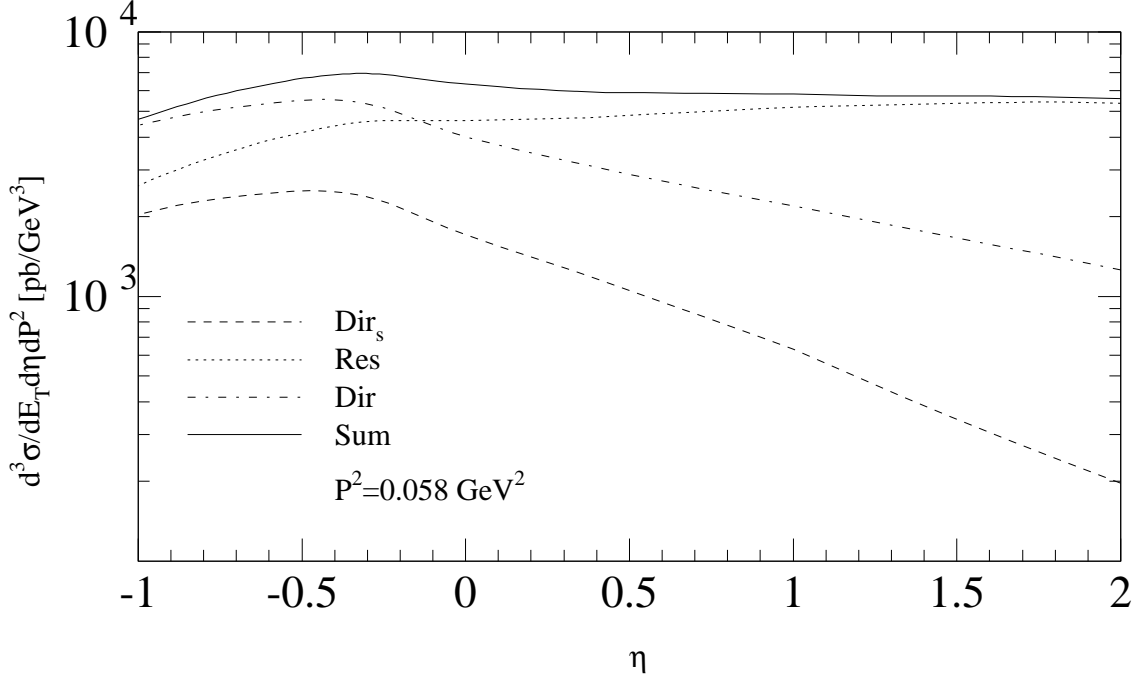


Figure 5a: Comparisons of single-jet inclusive cross sections for $E_T = 7$ GeV and the virtuality $P^2 = 0.058$ GeV². The $\overline{\text{MS}}$ -SaS1M parametrization with $N_f = 4$ is chosen. The solid line gives the sum of the subtracted direct and the resolved term. The dash dotted curve is the direct contribution without subtraction.

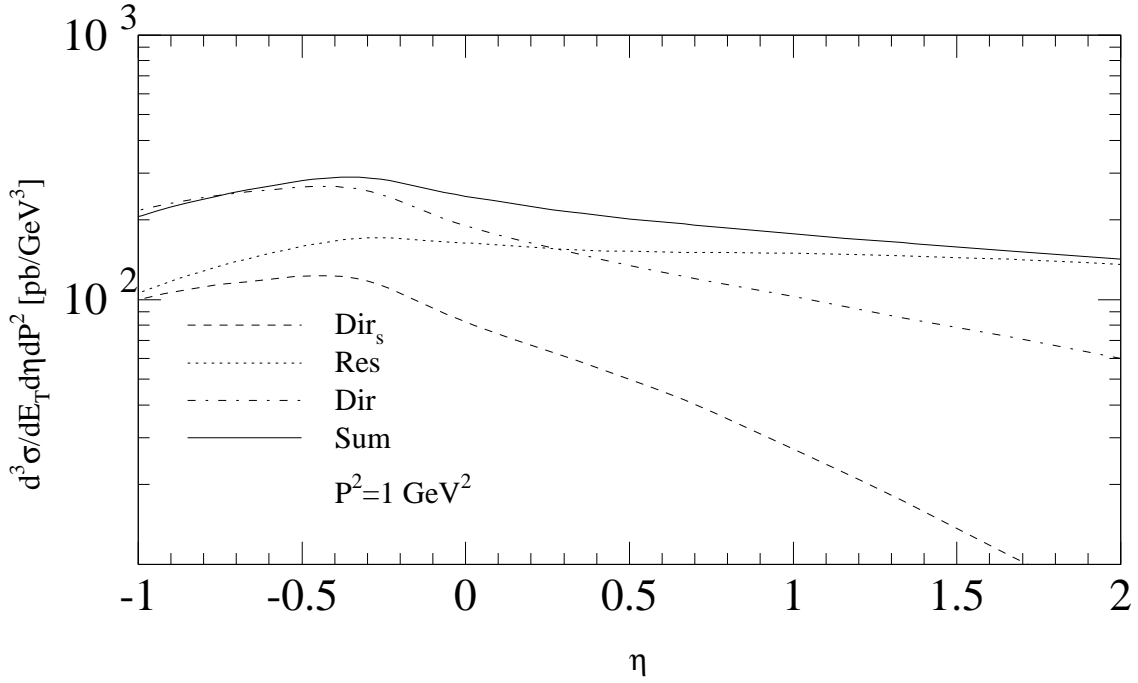


Figure 5b: Same as figure 5a with $P^2 = 1$ GeV².

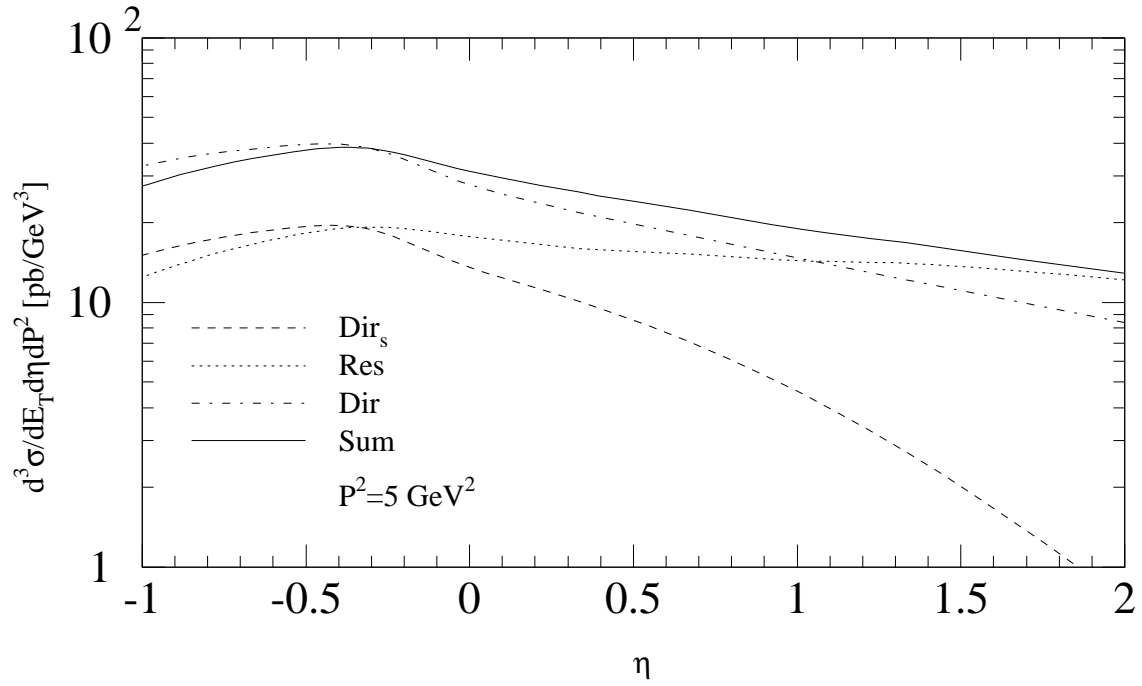


Figure 5c: Same as figure 5a with $P^2 = 5 \text{ GeV}^2$.

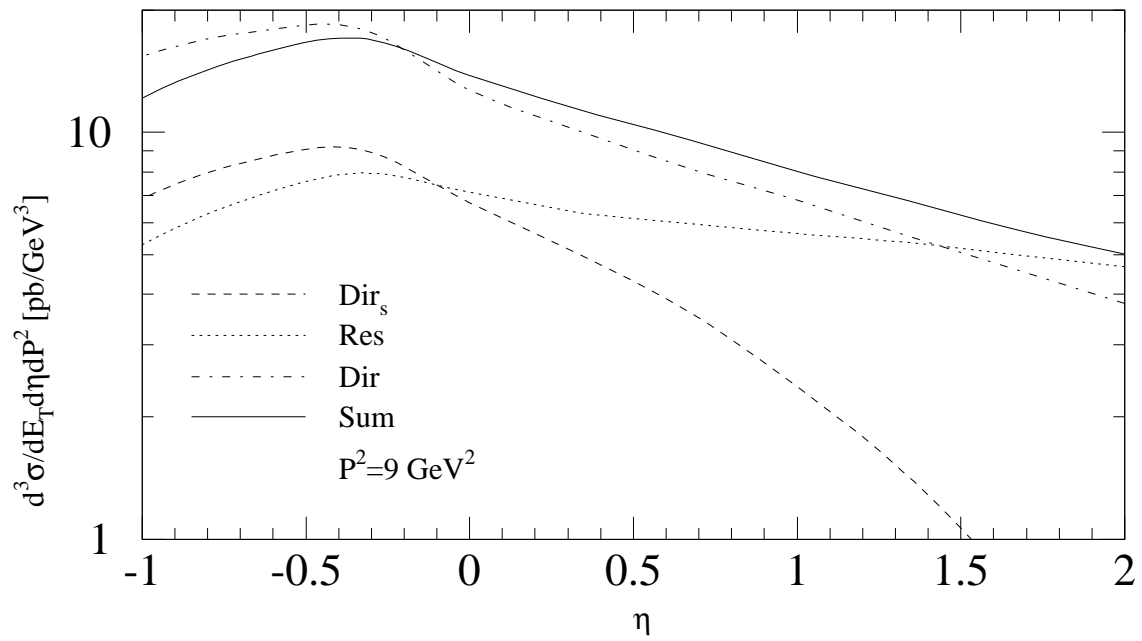


Figure 5d: Same as figure 5a with $P^2 = 9 \text{ GeV}^2$.

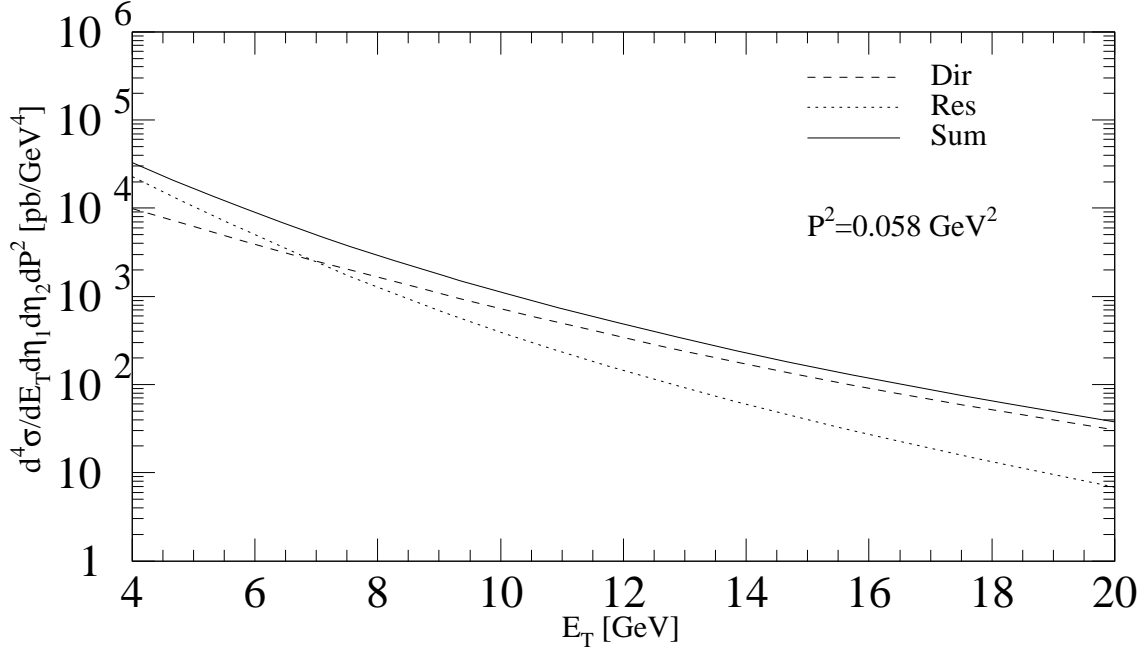


Figure 6a: Dijet inclusive cross section integrated over $\eta_1, \eta_2 \in [-1.125, 1.875]$ for the virtuality $P^2 = 0.058 \text{ GeV}^2$. The $\overline{\text{MS}}$ -GRS parametrization with $N_f = 3$ is chosen. The solid line is the sum of the direct and the resolved contribution. The dashed line is the direct-enriched contribution with $x_\gamma^{obs} > 0.75$ and the dotted curve is the resolved enriched contribution with $x_\gamma^{obs} < 0.75$.

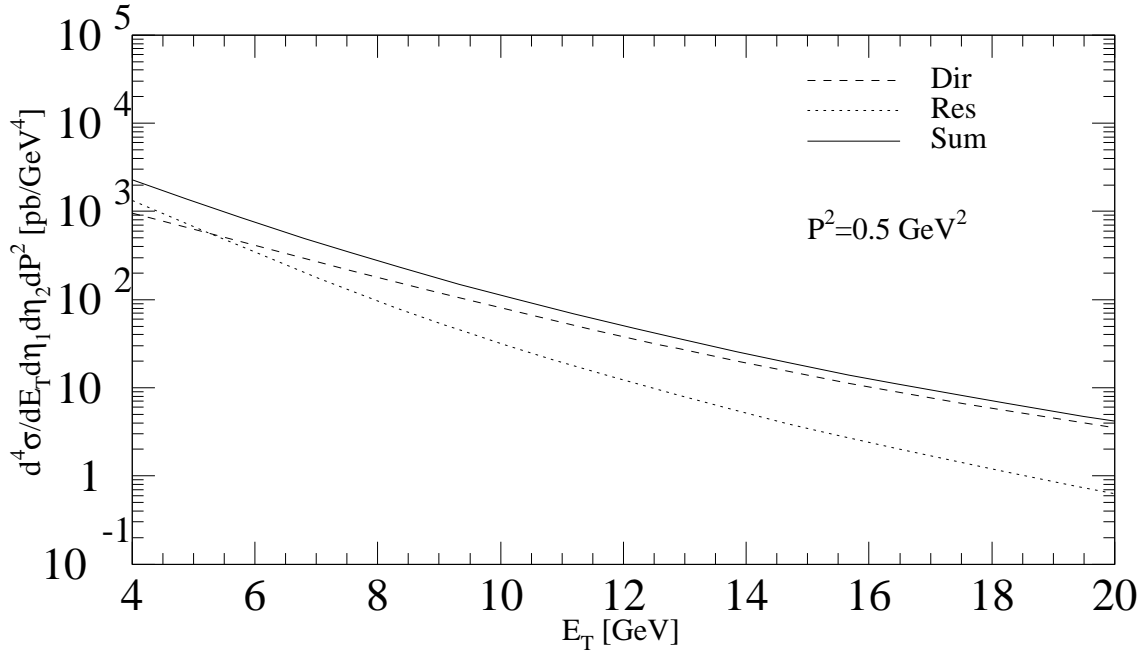


Figure 6b: Same as figure 6a with $P^2 = 0.5 \text{ GeV}^2$.

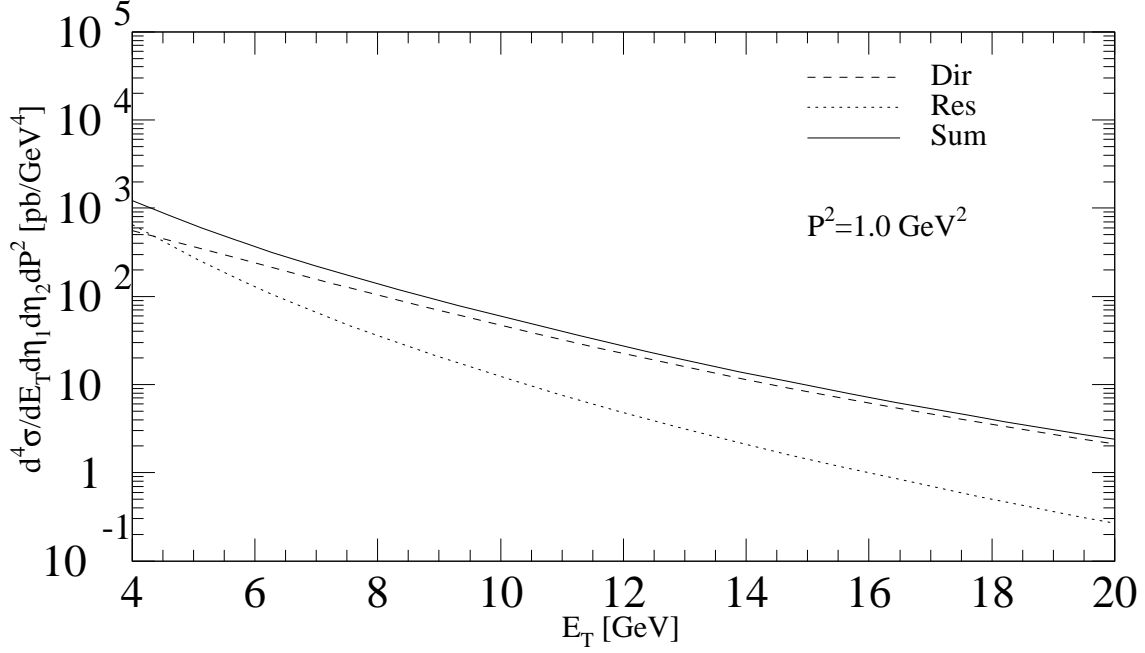


Figure 6c: Same as figure 6a with $P^2 = 1.0 \text{ GeV}^2$.

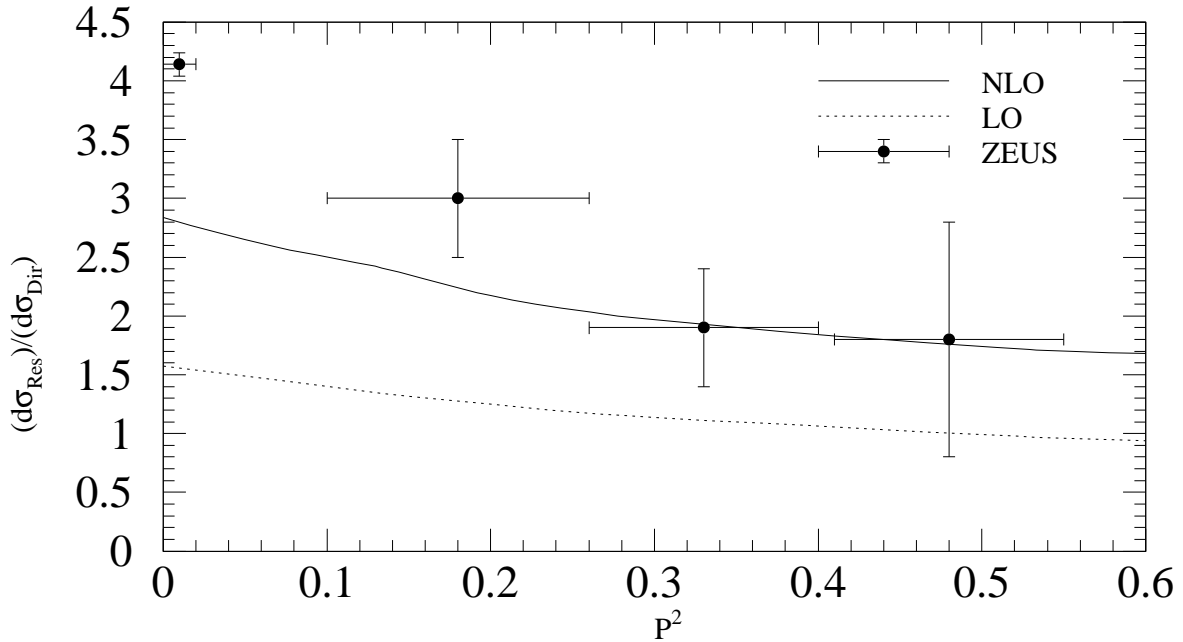


Figure 7: The ratio of the resolved-enriched to the direct-enriched contributions as calculated in Fig. 6a, b, c, integrated over $E_{T_1}, E_{T_2} > 4 \text{ GeV}$ in LO (dotted) and NLO (full) for the SaS1M parametrization with $N_f = 4$ compared with ZEUS data.